

Quasi-Wavefront Selection Algorithm for Fast and Accurate Ultra-Wideband Imaging with Polar Revised Range Point Migration

Takuya Sakamoto*, Toru Sato,
Graduate School of Informatics
Kyoto University
Yoshida-Honmachi, Sakyo-ku
Kyoto 606-8501, Japan

Rahmi Salman, Ingolf Willms,
Fachgebiet Nachrichtentechnische Systeme
Universitat Duisburg-Essen
Duisburg, Germany

Alexander G. Yarovoy
Microwave Sensing, Signals and Systems
Delft University of Technology
Mekelweg 4, 2628 CD
Delft, The Netherlands

Abstract—Ultra-wide-band sensing is an important technology for imaging in situations where conventional camera-based systems are difficult to use because of dense smoke or steam. Although many applications of such systems require real-time operation, conventional imaging algorithms cannot satisfy this demand, because most methods have focused on the imaging quality alone. Recently, a fast imaging algorithm, called polar revised range point migration (PRRPM), was developed that enabled the target images to be obtained within a short time. The PRRPM uses a closed-form transform called the polar inverse boundary scattering transform (PIBST), which expresses the relationship between the signal delay time and the target images. Although the PIBST was shown to be capable of producing images quickly, the images were degenerated because of wrongly estimated delay times, especially if the fractional bandwidth was narrow, and generated ringing waveforms with multiple false peaks. In this paper, we propose a method to select the correct delay times among multiple peaks that were estimated using the conventional method, which suppresses the false images caused by the ringing components. The proposed method is applied to measurements with m-sequence radar to establish the performance of the method.

I. INTRODUCTION

Ultra-wide-band (UWB) imaging technology has been attracting increasing attention because it has immense potential for security-related applications, such as surveillance systems and autonomous rescue robotics. One necessary condition for the imaging algorithms in such applications is fast computational speed, because real-time operation is required. Various imaging methods for UWB radar have been developed [1]-[6]. However, many of the existing imaging methods do not fulfill the fast computation requirements.

One method developed to meet this need was the revised range point migration (RRPM) method [7], [8] for antennas scanning along a straight line or on a plane. The RRPM is based on a reversible transform, the inverse boundary scattering transform (IBST) [9]-[12], and weighted averaging of multiple signal peaks to estimate stable derivatives. The RRPM was further extended to polar coordinates, to produce the polar revised range point migration (PRRPM) method [13]. The PRRPM also uses a closed-form transform, the

polar IBST (PIBST), which depicts the relationship between the target shape and the received signals obtained with an antenna scanning along a circle. Both the RRPM and PRRPM methods can obtain images even for complex-shaped targets under noisy conditions.

When using these transform-based imaging algorithms, it is assumed that a single range is estimated for each target-background interface. However, the conventional methods give multiple ranges for signals with bandwidths narrower than 100%, because the ringing waveforms have multiple peaks, which degrades the image quality. Salman and Willms proposed a method to estimate quasi-wavefronts by using a matched filter with a synthetic waveform formed by the summation of overlapping template waveforms [14]. Although the method is effective for estimation of the correct quasi-wavefronts, the method is based on repetitive filtering with various combinations of multiple parameters, which increases the computation load and degrades the fast computation capability of the PRRPM method.

In this paper, we propose a selection method for quasi-wavefronts that gives the correct quasi-wavefronts for each wave packet, resulting in a better quality imaging capability. Because the method does not require repetitive computation, the method maintains the fast computational speed of the PRRPM method. We performed measurements using a maximum length binary sequence (m-sequence) UWB radar system with a metallic target on a rotating platform to assess the performance of the proposed method.

II. SYSTEM MODEL

We use two-dimensional polar coordinates in the imaging plane for our UWB imaging system. Fig. 1 shows a schematic of the system model. The device is a mono-static radar system that uses a single antenna as both transmitter and receiver. The antenna is positioned on a ring of radius R , centered on the origin of the coordinate system. Based on the azimuth angle θ , the location of the antenna is expressed as $(x, y) = (R \cos \theta, R \sin \theta)$. The targets are placed within the circular trajectory of the scanning antenna. UWB pulses are

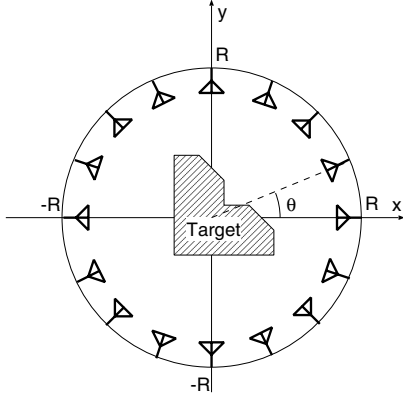


Fig. 1. System model with a circular antenna array surrounding a target.

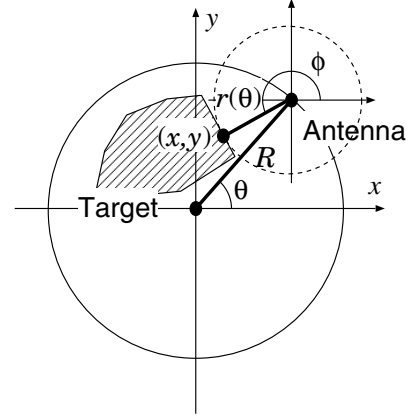


Fig. 2. Relationship between variables defined in the system model.

transmitted and the echoes are received. The received signals contain not only the echoes from the target but also a coupling signal and background clutter. To eliminate these unnecessary signals, the background signal, measured without the target prior to the actual measurements, can be subtracted from the received signal. Given the antenna location corresponding to the angle θ , the received signal after applying the matched filter is then denoted by $s(\theta, r)$ with $r = ct/2$, where c is the speed of the electromagnetic wave and t is the time interval between transmission and reception.

III. CONVENTIONAL QUASI-WAVEFRONT EXTRACTION

To estimate the target shape, many conventional imaging methods use back propagation to form the image. This is also called migration. The processing is time-consuming because the propagation paths must be calculated repeatedly. To overcome this difficulty, we developed a closed-form transform that is used to obtain images from the range as a function of the angle of the antenna position that is called a quasi-wavefront. The procedure begins with estimation of the quasi-wavefronts.

First, we extract the peaks of the received signals, which satisfy

$$\frac{\partial}{\partial r} s(\theta, r) = 0, \quad (1)$$

$$|s(\theta, r)| > T_s, \quad (2)$$

where T_s is a constant threshold introduced to filter out noise. These peaks are indexed as (θ_i, r_i) for $(i = 1, 2, \dots, N)$. The corresponding amplitudes of these peaks are, for simplicity, denoted by $s_i = s(\theta_i, r_i)$. For a single target with a simple shape, these points can easily be connected sequentially to form the curved lines of $r(\theta)$. The resulting function is called a quasi-wavefront. Ideally, the function $r(\theta)$ corresponds to the actual range between the target and the antenna. However, for a signal with a limited bandwidth, the resulting $r(\theta)$ has multiple values for the same target boundary caused by the ringing waveforms. This issue will be addressed in later sections.

IV. POLAR INVERSE SCATTERING TRANSFORM FOR IMAGING

We assume that the target has a clear boundary between the background and the target medium. In the previous section, we calculated the function $r(\theta)$ that gives the distance between the antenna and the scattering point on the boundary. The target boundary is then expressed in polar coordinates as

$$\begin{pmatrix} x \\ y \end{pmatrix} = R \begin{pmatrix} \cos \theta \\ \sin \theta \end{pmatrix} + r(\theta) \begin{pmatrix} \cos \phi \\ \sin \phi \end{pmatrix}, \quad (3)$$

where ϕ is the angle of the scattering point as seen from the viewpoint of the antenna. The actual target shape is expressed as follows [13]:

$$\phi = -\sin^{-1} \left(\frac{dr/d\theta}{R} \right) + \theta. \quad (4)$$

If r and $dr/d\theta$ are measured, the target image can then be calculated using Eqs. (3) and (4). In this way, the target can be imaged using this transform without any iteration, increasing the image processing speed. We call the transform defined by Eqs. (3) and (4) the PIBST. The relationship between the variables defined above is shown in Fig. 4.

V. POLAR REVISED RANGE POINT MIGRATION

The most significant issue with the algorithm described in the previous section is that the derivative $dr/d\theta$ is quite sensitive to noise and interference. The whole process depends on the assumption that the quasi-wavefront $r(\theta)$ can be estimated accurately, while the actual measurement is prone to various undesirable effects including noise, clutter, and overlapping multiple scattering waves. This issue makes it difficult to apply the PIBST alone to targets with complex shapes under noise- and clutter-rich conditions.

Therefore, we use a stable method, the RRPM, to estimate derivatives to mitigate the instability of the PIBST. Using a weighted average function, the relative orientation of the peaks around the i -th peak can be estimated as:

$$\psi_i = \frac{\sum_{j \neq i} w_{i,j} \tan^{-1} \left(\frac{r_i - r_j}{\theta_i - \theta_j} \right)}{\sum_{j \neq i} w_{i,j}}, \quad (5)$$

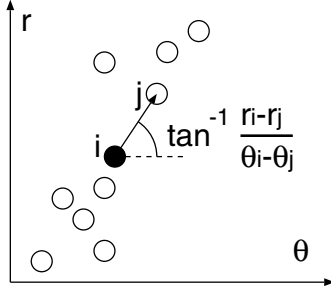


Fig. 3. Schematic of the RRPM method.

where

$$w_{i,j} = |s_i s_j| \exp\left(-\frac{(\theta_i - \theta_j)^2}{\sigma_\theta^2} - \frac{(r_i - r_j)^2}{\sigma_r^2}\right) \quad (6)$$

and $\left|\tan^{-1}\left(\frac{r_i - r_j}{\theta_i - \theta_j}\right)\right| < \pi/4$, and the summations are performed over pairs of peaks with the same sign in the 2nd derivative i. e.

$$s_{rr}(\theta_i, r_i) s_{rr}(\theta_j, r_j) > 0, \quad (7)$$

where $s_{rr} = \frac{\partial^2}{\partial r^2} s$. Figure 3 shows a schematic of the procedure in the RRPM method. As shown in the figure, the inclination of the points around the i -th point is calculated by averaging the angle between the i -th and j -th points over all j close to the i -th point. By finding ψ_i by using Eq. (5), we obtain an estimate of the quasi-wavefront orientation. We then calculate the derivative $dr/d\theta|_{\theta=\theta_i} = \tan(\psi_i)$. Finally, we substitute r and $dr/d\theta$ into the PIBST in Eqs. (3) and (4) to obtain the target image.

VI. PROPOSED QUASI-WAVEFRONT SELECTION

The conventional method used to estimate the quasi-wavefronts erroneously estimates multiple quasi-wavefronts for each echo if the fractional bandwidth is narrow, which results in ringing waveforms with multiple peak points. In this section, we propose a method to select the correct wavefronts from the wavefronts that were extracted in the previous section. This method uses the fact that the dominant quasi-wavefront has adjacent peaks with smaller absolute amplitudes but the opposite sign. Also, these adjacent peaks must be located at a specific distance from the main quasi-wavefront, where the distance corresponds to half the wavelength of the carrier frequency. If these conditions are satisfied, then the quasi-wavefront can be used to form an image.

For each θ , peaks are extracted as $r_1(\theta), r_2(\theta), \dots, r_N(\theta)$, where the range values are arranged in ascending order as $r_1(\theta) < r_2(\theta) < \dots < r_N(\theta)$. If the following conditions are

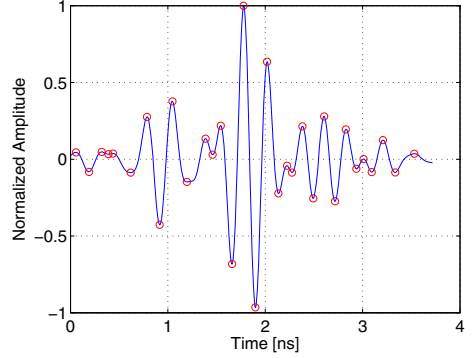


Fig. 4. Peak points extracted from a signal using the conventional method.

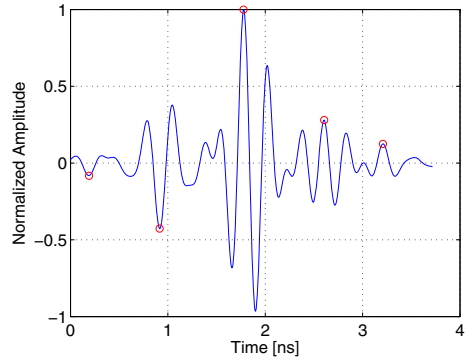


Fig. 5. Selected peak points extracted using the proposed method.

satisfied, then $r_n(\theta)$ is used for imaging.

$$|r_n(\theta) - r_{n-1}(\theta) - r_c| < \delta, \quad (8)$$

$$|r_{n+1}(\theta) - r_n(\theta) - r_c| < \delta, \quad (9)$$

$$(1 + \epsilon)|s(\theta)_n| > |s(\theta)_{n-1}|, \quad (10)$$

$$(1 + \epsilon)|s(\theta)_n| > |s(\theta)_{n+1}|, \quad (11)$$

$$s(\theta)_n s(\theta)_{n-1} < 0, \quad (12)$$

$$s(\theta)_n s(\theta)_{n+1} < 0, \quad (13)$$

where δ and ϵ are small numbers that were chosen empirically. In the following applications, we assume that $\delta = 0.1$ cm and $\epsilon = 0.1$. Please note that δ should be much smaller than the wavelength of the central frequency. For larger δ and ϵ , the noise tolerance of the proposed algorithm improves, while the number of false images increases.

Figures 4 and 5 show examples of the conventional and proposed methods for quasi-wavefront estimation, respectively. For this comparison, we set the threshold $T_s = 0$ for simplicity. In Fig. 4, all the local maxima and minima are estimated, whereas in Fig. 5, only the dominant peak point is chosen for each wave packet.

Figures 6 and 7 show the received signals at each antenna position on a circle where $0 \leq \theta \leq 360^\circ$ and the quasi-wavefronts extracted using the conventional method with thresholds $T_s = 0.1A_{\max}$ and $T_s = 0.3A_{\max}$, respectively,

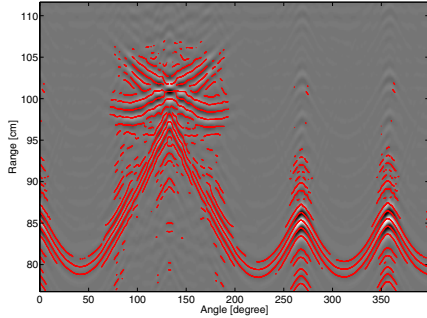


Fig. 6. Quasi-wavefronts extracted using the conventional method with $T_s = 0.1A_{\max}$.

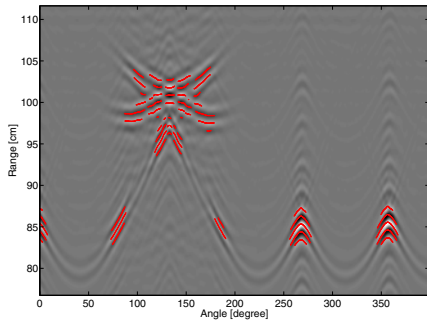


Fig. 7. Quasi-wavefronts extracted using the conventional method with $T_s = 0.3A_{\max}$.

where A_{\max} is the maximum signal amplitude. As shown in Fig. 6, the conventional method extracts multiple peaks for a single target boundary. This is because the number of cycles in the wave packet is approximately equal to the inverse of the fractional band width. The actual waveforms in this case have a fractional bandwidth of 69%, causing ringing and multiple peaks in the waveforms. Figure 7 shows that the conventional method still extracts multiple peaks even when a higher threshold is set to prevent insignificant peaks from being picked up. In this image, we see that the threshold $T_s = 0.3A_{\max}$ is too high to extract edge diffraction waves, while it is too low to prevent specular reflection waves. This is because the echo intensities of the specular reflection and the edge diffraction are quite different. It is therefore impossible to filter out the ringing peaks by adjusting the threshold alone.

Figure 8 shows the same figure where the quasi-wavefronts were extracted using the proposed method. The threshold is set as $T_s = 0.1A_{\max}$, which is the same as that in Fig. 6. The figure clearly shows that the proposed method is effective in preventing multiple peaks from being picked up from a single waveform. Because of waveform distortion, the proposed method can extract inconsistent range values in some places. However, the proposed method generally estimates the quasi-wavefronts successfully in most parts of the signals.

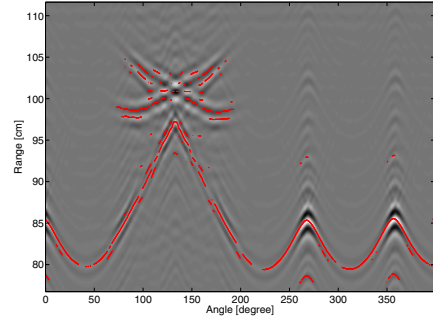


Fig. 8. Quasi-wavefronts extracted using the proposed method with $T_s = 0.1A_{\max}$.

VII. APPLICATION TO MEASUREMENT DATA

We conducted measurements to investigate the performance of the proposed imaging algorithm. We used an m-sequence UWB radar system [15], [16] with a DC-4.5 GHz operating band. We combined this system with a 9 GHz carrier signal generator to up-convert and generate signals with a frequency band from 4.5 GHz to 13.5 GHz, with a bandwidth of 9 GHz giving a maximum fractional bandwidth of 100%. It should be noted that the actual fractional bandwidth of the received signals is 69% which is narrower than that of the original waveform generated by the pulse generator, because of the frequency characteristics of the antennas and the circuits, including the matching of the antennas and cables. In assembling a bi-static radar system, we mounted a pair of directive Teflon-embedded tapered slot line Vivaldi antennas [15], [17] with 10 cm antenna separation to mitigate the antenna cross-talk. The antenna gain is 15 dBi, and the beam width is 25 degrees.

The target objects are metallic pillars with uniform horizontal cross-sections (Fig. 9); the model is considered to be approximately two-dimensional. Each target is placed in turn on a rotating platform with an axis that is 100 cm away from the midpoint of the antennas, giving $R = 100.0$ cm. The table rotates through 360 degrees in 1-degree steps, giving 360 measuring points. The rotation is electrically controlled with an accurate stepping motor. The details of the measurement setup are given in [18] and [16]. The imaging was performed for the same measurement data set using conventional imaging methods [15], [17], [18], [19]. We set the parameters for the proposed method to be $T_s = 0.1A_{\max}$, $\sigma_\theta = 0.5^\circ$ and $\sigma_r = 0.05$ cm. We first extracted 15 quasi-wavefronts for each measurement angle using the conventional quasi-wavefront extraction method. Then, we applied the proposed quasi-wavefront selection method.

For comparison, we first generated images using the conventional diffraction stack migration as shown in Figs. 10 and 11. To make the comparison fair, we calculated the image only if the signal amplitude was larger than the threshold $T_s = 0.1A_{\max}$ which is the value used for the proposed method. The computation using the migration method took 18.6 s and 19.4 s for targets A and B respectively. Figures 12

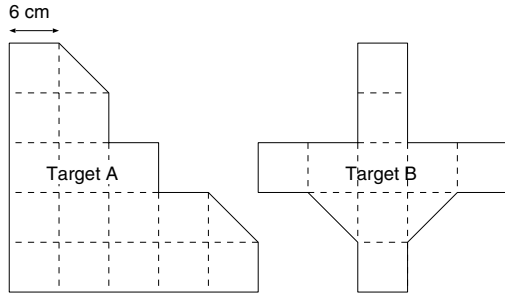


Fig. 9. Target shapes used in the measurements.

and 13 show the images generated using the PRRPM method with a conventional quasi-wavefront extraction method. The results show that the PRRPM method can also generate target images, although they are blurred because of the multiple peaks caused by the ringing components in the received signals.

Figures 14 and 15 show the images generated using the PRRPM with the proposed quasi-wavefront selection method. It is shown that the image degradation is suppressed by the proposed method, giving clearer and more accurate images compared with those of the conventional migration or PRRPM methods. The total imaging process using the proposed method took only 0.57 s and 0.75 s for targets A and B respectively; these times are 32 and 25 times shorter than those achieved using the conventional migration method for targets A and B respectively. To compare the computation times, we used a 64-bit version of Matlab 2012b running on a laptop with an Intel Core i7-3610QM CPU with 2.30 GHz clock speed and 4.0 GB of RAM.

VIII. DISCUSSION

The proposed method can be applied to dielectric objects as well as metallic objects. In this case, however, the resulting image in general will contain artifacts caused by multiple reflections between the interface between the dielectric material and air. If the conductivity and permittivity of the material are large enough, this multiple reflection effect is negligible. It is an important task to revise the proposed method to mitigate this kind of false image.

IX. CONCLUSION

In this paper, we proposed a selection method for quasi-wavefronts, which are functions that express the relationship between range and antenna motion, which is important for imaging with UWB sensing systems. The complete algorithm consists of the proposed method used together with the PRRPM method, which is known to be able to generate images quickly for radar with a circularly scanning antenna. The proposed method chooses quasi-wavefronts that have adjacent peaks with a lower and opposite amplitude, giving a single quasi-wavefront for a single echo. The performance of the proposed method incorporated into the PRRPM method has been investigated experimentally using an m-sequence

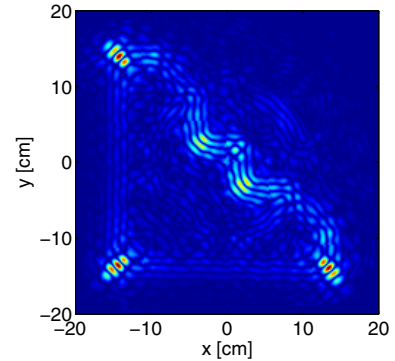


Fig. 10. Estimated target shape using the conventional migration method for target A.

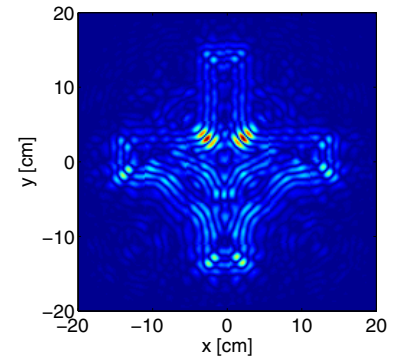


Fig. 11. Estimated target shape using the conventional migration method for target B.

radar system and metallic targets on a rotating platform. The imaging results show that the proposed method can generate clear images; while maintaining fast computation speeds. The computation times of the proposed method were found to be 32 and 25 times shorter than those for the conventional migration method for two test measurements.

ACKNOWLEDGEMENT

This study was supported in part by the Japan Society for the Promotion of Science (JSPS) Postdoctoral Fellowships for Research Abroad (High-resolution imaging for human bodies with UWB radar using multipath echoes).

REFERENCES

- [1] X. Zhuge, A. G. Yarovoy, T. Savel'yev, L. Lighthart, "Modified Kirchhoff migration for UWB MIMO array-based radar imaging" IEEE Transactions on Geoscience and Remote Sensing, vol. 48, no. 6, pp. 2692–2703, 2010.
- [2] X. Zhuge, and A. Yarovoy, "A sparse aperture MIMO-SAR based UWB imaging system for concealed weapon detection," IEEE Transactions on Geoscience and Remote Sensing, vol. 49 no. 1, pp. 509–518, 2011.
- [3] Y. Wang, Y. Yang, A. E. Fathy, "Experimental assessment of the cross coupling and polarization effects on ultra-wide band see-through-wall imaging reconstruction," IEEE MTT-S International Microwave Symposium Digest, pp. 9–12, June 2009.
- [4] A. Nelander, "Switched array concepts for 3-D radar imaging," Proc. 2010 IEEE Radar Conference, pp. 1019–1024, 2010.

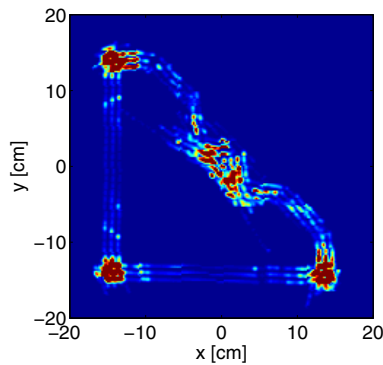


Fig. 12. Estimated target shape using the PRRPM method for target A.

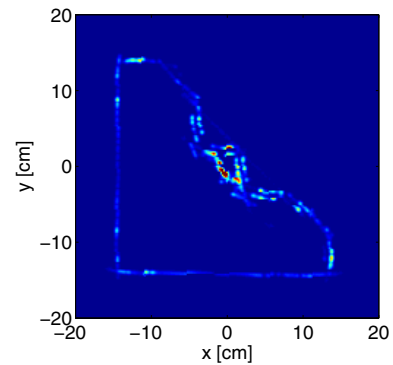


Fig. 14. Estimated target shape using the proposed method for target A.

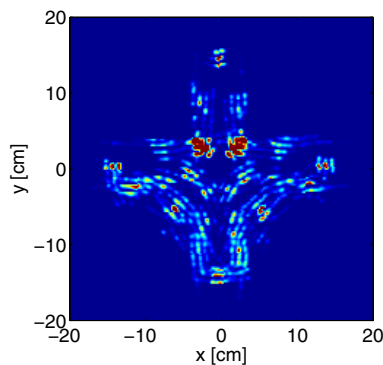


Fig. 13. Estimated target shape using the PRRPM method for target B.

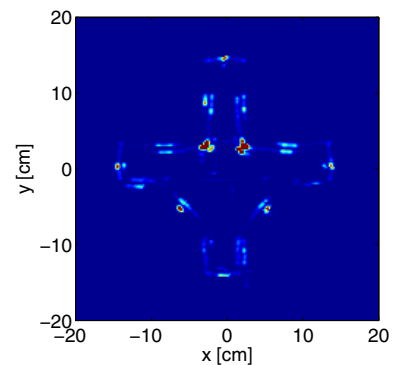


Fig. 15. Estimated target shape using the proposed method for target B.

- [5] T. Counts, A. C. Gurbuz, W. R. Scott Jr., J. H. McClellan, and K. Kim, "Multistatic ground-penetrating radar experiments," *IEEE Trans. Geoscience and Remote Sensing*, vol. 45, no. 8, pp. 2544–2553, Aug. 2007.
- [6] Y. Yang and A. E. Fathy, "Development and implementation of a real-time see-through-wall radar system based on FPGA," *IEEE Trans. Geoscience and Remote Sensing*, vol. 47, no. 5, pp. 1270–1280, May 2009.
- [7] T. Sakamoto, T. G. Savelyev, P. J. Aubry, and A. G. Yarovoy, "Revised Range Point Migration Method for Rapid 3-D Imaging with UWB Radar," *Proc. 2012 IEEE International Symposium on Antennas and Propagation and USNC-URSI National Radio Science Meeting*, July 2012.
- [8] T. Sakamoto, T. G. Savelyev, P. J. Aubry, and A. G. Yarovoy, "Fast Range Point Migration Method for Weapon Detection using Ultra-Wideband Radar," *Proc. European Radar Conference*, Nov. 2012.
- [9] T. Sakamoto, "A fast algorithm for 3-dimensional imaging with UWB pulse radar systems," *IEICE Trans. on Communications*, vol. E90-B, no. 3, pp. 636–644, 2007.
- [10] S. Hantscher, A. Reizenhahn, C. G. Diskus, "Through-Wall Imaging With a 3-D UWB SAR Algorithm," *IEEE Signal Processing Letters*, vol. 15, pp. 269–272, 2008.
- [11] R. Salman, I. Willms, "In-Wall Object Recognition based on SAR-like Imaging by UWB-Radar," *Proc. 8th European Conference on Synthetic Aperture Radar (EUSAR)*, 2010.
- [12] S. Kidera, Y. Kani, T. Sakamoto and T. Sato, "A fast and high-resolution 3-D imaging algorithm with linear array antennas for UWB pulse radars," *IEICE Trans. on Communications*, vol. E91-B, no. 8, pp. 2683–2691, 2008.
- [13] T. Sakamoto, T. Sato, R. Salman, I. Willms and A. G. Yarovoy, "Novel transform for ultra wide-band radar imaging with circular scanning antennas," *Proc. European Radar Conference 2013* (under review).
- [14] R. Salman and I. Willms, "Joint efficiency and performance enhancement of wavefront extraction algorithms for short-range super-resolution UWB radar," *Proc. 2012 The 7th German Microwave Conference (GeMiC)*, 2012.
- [15] R. Zetik, H. Yan, E. Malz, S. Jovanoska, G. Shen, R.S. Thomä, R. Salman, T. Schultze, R. Tobera, I. Willms, L. Reichardt, M. Janson, T. Zwick, W. Wiesbeck, T. Deißler, J. Thielecke, "Cooperative Localization and Object Recognition," *UKoLoS Ultra-Wideband Radio Technologies for Communications, Localization and Sensor Applications*, InTech Academic Publisher, ISBN: 978-953-307-740-6.
- [16] R. Salman and I. Willms, "Super-Resolution Object Recognition Approach for Complex Edged Objects by UWB Radar," *Object Recognition*, Intech.
- [17] R. Salman, I. Willms, L. Reichardt, T. Zwick and W. Wiesbeck, "On polarization diversity gain in short range UWB-Radar object imaging," *Proc. 2012 IEEE International Conference on Ultra-Wideband*, pp. 402–406, Sep. 2012.
- [18] R. Salman and I. Willms, "3D UWB radar super-resolution imaging for complex objects with discontinuous wavefronts," *Proc. 2011 IEEE International Conference on Ultra-Wideband*, Sep. 2011.
- [19] R. Salman and I. Willms, "A mobile security robot equipped with UWB-radar for super-resolution indoor positioning and localisation applications," *Proc. Indoor Positioning and Indoor Navigation*, Nov. 2012.